

# Positive-, Negative-, and Orthogonal-Phase-Velocity Propagation of Electromagnetic Plane Waves in a Simply Moving Medium

Tom G. Mackay<sup>1</sup>

*School of Mathematics, University of Edinburgh, Edinburgh EH9 3JZ, UK*

Akhlesh Lakhtakia

*CATMAS — Computational & Theoretical Materials Sciences Group*

*Department of Engineering Science and Mechanics*

*Pennsylvania State University, University Park, PA 16802-6812, USA*

Sandi Setiawan

*School of Mathematics, University of Edinburgh, Edinburgh EH9 3JZ, UK*

## Abstract

Planewave propagation in a simply moving, dielectric-magnetic medium that is isotropic in the co-moving reference frame, is classified into three different categories: positive-, negative-, and orthogonal-phase-velocity (PPV, NPV, and OPV). Calculations from the perspective of an observer located in a non-co-moving reference frame show that, whether the nature of planewave propagation is PPV or NPV (or OPV in the case of nondissipative mediums) depends strongly upon the magnitude and direction of that observer's velocity relative to the medium. PPV propagation is characterized by a positive real wavenumber, NPV propagation by a negative real wavenumber. OPV propagation only occurs for nondissipative mediums, but weakly dissipative mediums can support nearly OPV propagation.

**Keywords:** Minkowski constitutive relations, phase velocity, Poynting vector

## 1 Introduction

Although the complexity of the response of materials to electromagnetic radiation has long been recognized, the subdiscipline of *complex-mediums electromagnetics* (CME) came into prominence only during the 1990s — as Weiglhofer recently demonstrated in an extended review [1]. Besides nonlinearity, general complex mediums are not merely anisotropic, but are also magnetoelectric. Plasmas, ferrites, isotropic chiral materials, structurally chiral

---

<sup>1</sup>Corresponding Author. Fax: + 44 131 650 6553; e-mail: T.Mackay@ed.ac.uk.

materials, bianisotropic materials — all are excellent examples of linear complex mediums. Some of these materials occur in nature, others are artificially made. Add nonlinearity to the mix, and a bewilderingly huge palette of electromagnetic response properties emerges [2, 3].

While that stream of CME continues to flow unabated, a second stream of CME sprang in 2000. This new stream initially contained quite simple mediums: isotropic and dielectric–magnetic, but with the phase velocity of plane waves therein being in opposition to the time–averaged Poynting vector [4]. There has been some intermingling of the two streams [5, 6], but much of today’s focus in the second stream is still on isotropic and dielectric–magnetic mediums.

One current in that stream is the visualization of the negative–phase–velocity (NPV) scenario by inertial observers that are moving at a fixed velocity with respect to a certain medium (or vice versa!). This is a sensible issue, as human vehicles continue to penetrate the universe beyond our planetary atmosphere [7]. In a predecessor paper [8], we theoretically demonstrated that isotropic dielectric–magnetic mediums which do not support NPV propagation when viewed by a co–moving observer, *can* support NPV propagation when they are viewed in a reference frame which is translating at a fixed velocity of sufficiently high magnitude. Even more recently, we deduced the possibility of orthogonal–phase–velocity (OPV) propagation — a phenomenon characterized by the orthogonality of the phase velocity and the time–averaged Poynting vector, when viewed by a non–co–moving inertial observer [9].

In this paper, we report a comprehensive study of NPV, OPV, and the conventional positive–phase–velocity (PPV) propagation of plane waves in a simply moving, homogeneous, dielectric–magnetic medium that is isotropic with respect to a co–moving observer. The plan of this paper is as follows: Section 2 is devoted to the Minkowski constitutive relations and planewave propagation. Section 3 contains numerical results for NPV, PPV, and OPV propagation in both dissipative and nondissipative mediums. Conclusions are presented in Section 4.

A note on notation:  $\text{Re}\{Q\}$  and  $\text{Im}\{Q\}$  represent the real and imaginary parts, respectively, of a complex–valued  $Q$ . The complex conjugate is written as  $Q^*$ . Vectors are identified by bold typeface and  $3\times 3$  dyadics are double underlined;  $\hat{\mathbf{v}}$  is a unit vector co–directional with  $\mathbf{v}$ ; the unit dyadic is  $\underline{\underline{I}}$ ; and  $\mathbf{r}$  denotes the spatial coordinate vector. The permittivity and permeability of free space (i.e., vacuum) are  $\epsilon_0$  and  $\mu_0$ , respectively;  $c_0 = (\epsilon_0\mu_0)^{-1/2}$  is the speed of light in free space;  $\omega$  is the angular frequency; and  $k_0 = \omega/c_0$ . An  $\exp(-i\omega t)$  time–dependence is implicit.

## 2 Theory

### 2.1 Minkowski constitutive relations

Let us consider a homogeneous, isotropic, dielectric–magnetic medium, characterized by its relative permittivity  $\epsilon_r$  and relative permeability  $\mu_r$ , in an inertial frame of reference  $\Sigma'$ .

That is, the frequency–domain constitutive relations

$$\left. \begin{aligned} \mathbf{D}' &= \epsilon_0 \epsilon_r \mathbf{E}' \\ \mathbf{B}' &= \mu_0 \mu_r \mathbf{B}' \end{aligned} \right\}, \quad (1)$$

describe the medium from the perspective of an observer located in  $\Sigma'$ .

The inertial reference frame  $\Sigma'$  moves at constant velocity  $\mathbf{v} = v \hat{\mathbf{v}}$  relative to another inertial reference frame  $\Sigma$ . From the perspective of an observer located in  $\Sigma$ , the medium is described by the Minkowski constitutive relations [10, 8]

$$\left. \begin{aligned} \mathbf{D} &= \epsilon_0 \epsilon_r \underline{\underline{\alpha}} \cdot \mathbf{E} + \frac{m \hat{\mathbf{v}} \times \mathbf{H}}{c_0} \\ \mathbf{B} &= -\frac{m \hat{\mathbf{v}} \times \mathbf{E}}{c_0} + \mu_0 \mu_r \underline{\underline{\alpha}} \cdot \mathbf{H} \end{aligned} \right\}, \quad (2)$$

where

$$\underline{\underline{\alpha}} = \alpha \underline{\underline{I}} + (1 - \alpha) \hat{\mathbf{v}} \hat{\mathbf{v}}, \quad (3)$$

$$\alpha = \frac{1 - \beta^2}{1 - \epsilon_r \mu_r \beta^2}, \quad (4)$$

$$m = \beta \frac{\epsilon_r \mu_r - 1}{1 - \epsilon_r \mu_r \beta^2}. \quad (5)$$

The transformation from (1) to (2) is achieved via

$$\mathbf{E}' = (\mathbf{E} \cdot \hat{\mathbf{v}}) \hat{\mathbf{v}} + \frac{1}{\sqrt{1 - \beta^2}} [(\underline{\underline{I}} - \hat{\mathbf{v}} \hat{\mathbf{v}}) \cdot \mathbf{E} + \mathbf{v} \times \mathbf{B}], \quad (6)$$

$$\mathbf{B}' = (\mathbf{B} \cdot \hat{\mathbf{v}}) \hat{\mathbf{v}} + \frac{1}{\sqrt{1 - \beta^2}} [(\underline{\underline{I}} - \hat{\mathbf{v}} \hat{\mathbf{v}}) \cdot \mathbf{B} - \frac{\mathbf{v} \times \mathbf{E}}{c_0^2}], \quad (7)$$

$$\mathbf{H}' = (\mathbf{H} \cdot \hat{\mathbf{v}}) \hat{\mathbf{v}} + \frac{1}{\sqrt{1 - \beta^2}} [(\underline{\underline{I}} - \hat{\mathbf{v}} \hat{\mathbf{v}}) \cdot \mathbf{H} - \mathbf{v} \times \mathbf{D}], \quad (8)$$

$$\mathbf{D}' = (\mathbf{D} \cdot \hat{\mathbf{v}}) \hat{\mathbf{v}} + \frac{1}{\sqrt{1 - \beta^2}} [(\underline{\underline{I}} - \hat{\mathbf{v}} \hat{\mathbf{v}}) \cdot \mathbf{D} + \frac{\mathbf{v} \times \mathbf{H}}{c_0^2}], \quad (9)$$

where  $\beta = v/c_0$ .

In the remainder of this paper, the propagation of plane waves in a medium described by the Minkowski constitutive relations (2) is investigated, with particular emphasis on the orientation of the phase velocity relative to the time–averaged Poynting vector. The reader is referred to standard works [10]–[12] for background details on planewave propagation within the context of special theory of relativity.

## 2.2 Planewave propagation

Plane waves in the chosen medium are described by the field phasors

$$\left. \begin{aligned} \mathbf{E} &= \mathbf{E}_0 \exp(i\mathbf{k} \cdot \mathbf{r}) \\ \mathbf{H} &= \mathbf{H}_0 \exp(i\mathbf{k} \cdot \mathbf{r}) \end{aligned} \right\}. \quad (10)$$

Our attention is restricted to uniform plane waves, as given by the wavevector  $\mathbf{k} = k \hat{\mathbf{k}}$  where the unit vector  $\hat{\mathbf{k}} \in \mathbb{R}^3$ . The wavenumber  $k$  is generally complex-valued, i.e.,

$$k = k_R + ik_I, \quad (11)$$

where  $k_R = \text{Re}\{k\}$  and  $k_I = \text{Im}\{k\}$ .

To calculate the wavenumbers, solutions of the form (10) are sought to the frequency-domain Maxwell curl postulates combined with the Minkowski constitutive relations. Thus, we find [8, 10]

$$k = k_0 \frac{-\beta\xi \hat{\mathbf{k}} \cdot \hat{\mathbf{v}} \pm \sqrt{\Delta}}{1 - \xi \left(\beta \hat{\mathbf{k}} \cdot \hat{\mathbf{v}}\right)^2}, \quad (12)$$

wherein

$$\xi = \frac{\epsilon_r \mu_r - 1}{1 - \beta^2}, \quad (13)$$

$$\Delta = 1 + (\epsilon_r \mu_r - 1) \delta, \quad (14)$$

$$\delta = \frac{1 - \left(\beta \hat{\mathbf{k}} \cdot \hat{\mathbf{v}}\right)^2}{1 - \beta^2} \geq 1. \quad (15)$$

Note that the medium with constitutive relations (2) is unirefringent since the two wavenumbers represented by (12) are not independent. The direction of planewave propagation determines the choice of sign for the square root term in (12).

The amplitudes of the electromagnetic field phasors may expressed as [8]

$$\mathbf{E}_0 = C_1 \mathbf{e}_1 + C_2 \mathbf{e}_2, \quad (16)$$

$$\mathbf{H}_0 = \frac{C_1}{\omega \mu_0 \mu_r} \mathbf{e}_2 - \omega \epsilon_0 \epsilon_r C_2 \mathbf{e}_1, \quad (17)$$

where  $C_1$  and  $C_2$  are arbitrary constants. The orthogonal eigenvectors  $\mathbf{e}_1$  and  $\mathbf{e}_2$  are given by

$$\mathbf{e}_1 = \mathbf{k} \times \hat{\mathbf{v}}, \quad (18)$$

$$\mathbf{e}_2 = \mathbf{a} \times \mathbf{e}_1, \quad (19)$$

with

$$\mathbf{a} = \mathbf{k} + \frac{\xi(\omega - \mathbf{k} \cdot \mathbf{v})}{c_0^2} \mathbf{v}. \quad (20)$$

Hence, the time-averaged Poynting vector

$$\langle \mathbf{P} \rangle = \frac{|\mathbf{e}_1|^2 \exp(-2k_I \hat{\mathbf{k}} \cdot \mathbf{r})}{2} \left( \frac{|C_1|^2}{\omega \mu_0} \mathbf{p}_1 + |C_2|^2 \omega \epsilon_0 \mathbf{p}_2 \right), \quad (21)$$

is delivered by (16)–(19), where

$$\left. \begin{aligned} \mathbf{p}_1 &= \operatorname{Re} \left\{ \frac{1}{\mu_r} \mathbf{a} \right\} \\ \mathbf{p}_2 &= \operatorname{Re} \{ \epsilon_r^* \mathbf{a} \} \end{aligned} \right\}. \quad (22)$$

The phase velocity

$$\mathbf{v}_p = c_0 \frac{k_0}{k_R} \hat{\mathbf{k}}, \quad (23)$$

is categorized in terms of its orientation relative to the time-averaged Poynting vector as follows:

- positive phase velocity (PPV) is characterized by  $\mathbf{v}_p \cdot \langle \mathbf{P} \rangle > 0$ ,
- negative phase velocity (NPV) is characterized by  $\mathbf{v}_p \cdot \langle \mathbf{P} \rangle < 0$ , and
- orthogonal phase velocity (OPV) is characterized by  $\mathbf{v}_p \cdot \langle \mathbf{P} \rangle = 0$ .

As described elsewhere, the phenomenon of OPV propagation arises for nondissipative mediums when  $\Delta < 0$  [9].

### 3 Numerical illustrations

Let us now explore numerically the occurrence of PPV, NPV, and OPV propagation within the parameter space provided by  $\{\epsilon_r, \mu_r, \mathbf{v}\}$ . The velocity vector  $\mathbf{v}$  is characterized by its relative magnitude  $\beta$  and its orientation angle  $\theta = \cos^{-1}(\hat{\mathbf{k}} \cdot \hat{\mathbf{v}})$  relative to the direction of planewave propagation, in the remainder of this paper.

#### 3.1 Wavenumber

We begin by considering the wavevector  $\mathbf{k}$ . Notice from (12) that the wavenumber  $k$  is a function of the product  $\epsilon_r \mu_r$ . In Figure 1, the real and imaginary parts of  $k$  are plotted for nondissipative mediums with  $\epsilon_r \mu_r \in (-10, 10)$ , for  $\beta \in \{0.3, 0.6, 0.9\}$  and the range of  $\theta$  values given in Table 1. The imaginary part of  $k$  is null-valued across much — but not all — of the range  $\epsilon_r \mu_r > 0$ .

Furthermore, at higher values of  $\beta$ ,  $k_I \neq 0$  for larger positive values of  $\epsilon_r \mu_r$ . This reflects the fact that  $\Delta$  can be either positive- or negative-valued for  $0 < \epsilon_r \mu_r < 1$ , depending upon the magnitude and direction of  $\mathbf{v}$ . Many schemes for materials satisfying the condition

$0 < \epsilon_r \mu_r < 1$  have been formulated [13, 14, 15], although we must note that dissipation then is hard to avoid.

The real part of  $k$  in Figure 1 becomes unbounded for  $\epsilon_r \mu_r > 1$ , at points at which the denominator  $(1 - \xi \beta^2 \cos^2 \theta)$  in (12) vanishes. In view of our interest in the transition between PPV and NPV propagation, it is significant that  $k_R$  changes sign as  $\epsilon_r \mu_r$  increases from  $-10$  to  $+10$  only for  $90^\circ < \theta < 180^\circ$ .

For dissipative mediums,  $\epsilon_r \in \mathbb{C}$  and  $\mu_r \in \mathbb{C}$ ; hence,  $\epsilon_r = \epsilon_r^R + i\epsilon_r^I$  and  $\mu_r = \mu_r^R + i\mu_r^I$ , where  $\epsilon_r^{R,I} \in \mathbb{R}$  and  $\mu_r^{R,I} \in \mathbb{R}$ . The wavenumber is plotted as a function of  $\epsilon_r^R \in (-10, 10)$  in Figure 2 — for  $\epsilon_r^I \in \{0.1|\epsilon_r^R|, 2|\epsilon_r^R|\}$ ,  $\mu_r = \pm 1 + 0.1i$ ,  $\beta = 0.9$  and the range of  $\theta$  values given in Table 1. Generally,  $k_I$  is nonzero for all values of  $\epsilon_r^R$ . As  $\epsilon_r^R$  varies, strong resonances are observed in Figure 2 for both  $k_R$  and  $k_I$ . Notice in Figure 2 that the real part of the wavenumber changes sign as  $\epsilon_r^R$  increases from  $-10$  to  $+10$  only for  $90^\circ < \theta < 180^\circ$ . This behaviour is similar to that observed for the nondissipative scenario illustrated in Figure 1.

### 3.2 Phase velocity

Let us now turn to nature of the phase velocity, as delineated by  $\mathbf{v}_p \cdot \langle \mathbf{P} \rangle$ . In Figure 3 the distribution of PPV, NPV, and OPV propagation is mapped out across the  $\beta\theta$  plane for nondissipative mediums with  $\epsilon_r \mu_r \in \{1/3, 2/3, 10/3\}$ . The OPV regime arises for  $\epsilon_r \mu_r < 1$  and for large values of  $\beta$ , spanning a range of values of  $\theta$  which are symmetrically distributed about  $\theta = 90^\circ$ . The NPV regime is restricted to  $\theta > 90^\circ$  for both  $\epsilon_r \mu_r < 1$  and  $\epsilon_r \mu_r > 1$ . We note that at  $\epsilon_r \mu_r = 1$ , the regions of NPV and OPV both vanish, in consonance with the Lorentz invariance of vacuum [11]. Planewave propagation for the nondissipative scenario corresponding to  $\epsilon_r \mu_r < 0$  (not shown in Figure 1) is OPV in nature for all values of  $\beta \in (0, 1)$ , since  $\Delta < 0$ .

For dissipative mediums, the distribution of the NPV and PPV regimes in the  $\beta\theta$  plane is displayed in Figure 4, for  $\epsilon_r^R \in \{\pm 1/3, \pm 2/3, \pm 10/3\}$ ,  $\epsilon_r^I \in \{0.1|\epsilon_r^R|, 2|\epsilon_r^R|\}$ , and  $\mu_r = \pm 1 + 0.1i$ . When  $\epsilon_r^R > 0$  and  $\mu_r^R > 0$ , propagation is predominantly PPV in nature, with the NPV regime limited to  $\theta > 90^\circ$  for large values of  $\beta$ . Similarly, for  $\epsilon_r^R < 0$  and  $\mu_r^R < 0$ , propagation is predominantly of the NPV type, with PPV propagation arising only for  $\theta < 90^\circ$  at large values of  $\beta$ . If  $\epsilon_r^R$  and  $\mu_r^R$  have different signs, and the imaginary parts of  $\epsilon_r$  and  $\mu_r$  are relatively small, then the distribution of NPV and PPV propagation is evenly divided in the  $\beta\theta$  plane along the line  $\theta = 90^\circ$ . This even split between the NPV and PPV regimes breaks down if the imaginary parts of  $\epsilon_r$  and/or  $\mu_r$  become sufficiently large.

We note, in particular, from Figure 4 that OPV propagation does not arise for dissipative mediums. Furthermore, there are no regions in the  $\beta\theta$  plane for which the sign of  $\mathbf{v}_p \cdot \langle \mathbf{P} \rangle$  is indeterminate; i.e., both  $\mathbf{v}_p \cdot \mathbf{p}_1$  and  $\mathbf{v}_p \cdot \mathbf{p}_2$  always have the same sign.

In order to explore the orientation of the vectors  $\mathbf{p}_1$  and  $\mathbf{p}_2$  relative to  $\mathbf{v}_p$ , let us introduce the angles

$$\phi_\ell = \cos^{-1} \left( \frac{\mathbf{v}_p \cdot \mathbf{p}_\ell}{|\mathbf{v}_p| |\mathbf{p}_\ell|} \right), \quad (\ell = 1, 2). \quad (24)$$

In Figure 5, contour plots of the angles  $\phi_1$  and  $\phi_2$  are shown in the  $\beta\theta$  plane for  $\epsilon_r^R = \pm 2/3$ ,

$\epsilon_r^I \in \{0.1|\epsilon_r^R|, 2|\epsilon_r^R|\}$ , and  $\mu_r = \pm 1 + 0.1i$ . We see that  $\phi_1 < 90^\circ$  and  $\phi_2 < 90^\circ$  for all values of  $\beta$  and  $\theta$ . Thus, the projection of the time-averaged Poynting vector onto  $\hat{\mathbf{k}}$  is always positive. Therefore, NPV propagation arises when  $k_R$  becomes negative-valued.

The vectors  $\mathbf{p}_1$  and  $\mathbf{p}_2$  are close to being perpendicular to  $\hat{\mathbf{k}}$  for large values of  $\beta$  when  $\theta$  takes values close to  $90^\circ$ , in Figure 5. This is most noticeable when the imaginary parts of  $\epsilon_r$  and  $\mu_r$  are relatively small. We infer that *nearly* OPV propagation is achieved for weakly dissipative mediums for large values of  $\beta$  when  $\theta$  is close to  $90^\circ$ . It is clear from Figure 5 that the orientations of  $\mathbf{p}_1$  and  $\mathbf{p}_2$  with respect to  $\hat{\mathbf{k}}$  are generally very similar. In particular, for weakly dissipative mediums, the orientations of  $\mathbf{p}_1$  and  $\mathbf{p}_2$  relative to  $\hat{\mathbf{k}}$  are almost the same across the entire  $\beta\theta$  plane.

The occurrences of NPV and PPV propagation are further explored in Figure 6, wherein the respective regimes are delineated as functions  $\epsilon_r^R \in (-10, 10)$  and  $\epsilon_r^I \in (0, 10)$  for  $\theta \in \{30^\circ, 150^\circ\}$ ,  $\beta \in \{0.1, 0.3, 0.5\}$ , and  $\mu_r = \pm 1 + 0.1i$ . When  $\theta > 90^\circ$  and  $\beta$  is small, the predominant type of propagation is PPV for values of  $\epsilon_r^R$  much less than zero but NPV for values of  $\epsilon_r^R$  much greater than zero. As  $\beta$  increases, the NPV regime expands, to the extent that when  $\beta = 0.5$  most of the  $\epsilon_r^R \epsilon_r^I$  plane supports NPV propagation. The reverse situation is observed when  $\theta < 90^\circ$ : planewave propagation becomes increasingly PPV in nature as  $\beta$  increases.

The relative orientation angles  $\phi_\ell$  of  $\mathbf{p}_\ell$ , ( $\ell = 1, 2$ ), corresponding to the NPV and PPV distributions presented in Figure 6, are provided in Figure 7. Both  $\phi_1$  and  $\phi_2$  are acute across the entire  $\epsilon_r^R \epsilon_r^I$  plane. Thus, our observation from Figure 5 that the projection of the time-averaged Poynting vector onto  $\hat{\mathbf{k}}$  is always positive, is further confirmed in Figure 7. Unlike the situation in Figure 5, the two vectors  $\mathbf{p}_1$  and  $\mathbf{p}_2$  clearly have quite different orientations when viewed as functions of  $\epsilon_r^R$  and  $\epsilon_r^I$ . Since  $\beta \leq 0.5$  and  $\theta$  is not close to  $90^\circ$ , the propagation represented in Figure 7 does not approximate to OPV in nature.

## 4 Conclusions

From our numerical studies, for a simply moving, dielectric-magnetic medium that is isotropic in the co-moving reference frame, we conclude the following.

- (i) Whether the nature of planewave propagation is PPV or NPV (or OPV in the case of nondissipative mediums) depends strongly upon the inertial frame of reference that the observer is situated in.
- (ii) The projection of the time-averaged Poynting vector onto the direction of planewave propagation, as given by  $\langle \mathbf{P} \rangle \cdot \hat{\mathbf{k}}$ , is non-negative. PPV propagation is characterized by  $k_R > 0$ ; NPV propagation arises when  $k_R$  becomes negative-valued.
- (iii) OPV propagation only occurs for nondissipative mediums; for such mediums it occurs when the imaginary part of the wavenumber is nonzero. Weakly dissipative mediums support nearly OPV propagation for large values of  $\beta$ , when  $\theta$  is close to  $90^\circ$ .

- (iv) The orientations of the component vectors  $\mathbf{p}_1$  and  $\mathbf{p}_2$  of the time-averaged Poynting vector are almost the same when viewed as functions of  $\beta$  and  $\theta$ , but the orientation of  $\mathbf{p}_1$  relative to  $\mathbf{p}_2$  is sensitively dependent upon the constitutive parameters  $\epsilon_r$  and  $\mu_r$ .

## References

- [1] W.S. Weiglhofer, Constitutive characterization of simple and complex mediums, in W.S. Weiglhofer, A. Lakhtakia (Eds.), Introduction to Complex Mediums for Optics and Electromagnetics, SPIE Press, Bellingham, WA, USA, 2003, pp. 27–61.
- [2] J.I. Gersten, F.W. Smith, The Physics and Chemistry of Materials, Wiley, New York, NY, USA, 2001.
- [3] W.S. Weiglhofer, A. Lakhtakia (Eds.), Introduction to Complex Mediums for Optics and Electromagnetics, SPIE Press, Bellingham, WA, USA, 2003.
- [4] A. Lakhtakia, M.W. McCall, W.S. Weiglhofer, Negative phase-velocity mediums, in W.S. Weiglhofer, A. Lakhtakia (Eds.), Introduction to Complex Mediums for Optics and Electromagnetics, SPIE Press, Bellingham, WA, USA, 2003, pp. 347–363.
- [5] J.B. Pendry (Ed.), Focus Issue: Negative Refraction and Metamaterials, Opt. Exp. 11 (2003). [http://www.opticsexpress.org/issue.cfm?issue\\_id=186](http://www.opticsexpress.org/issue.cfm?issue_id=186)
- [6] A. Lakhtakia, M. McCall (Eds.), Focus on Negative Refraction, New J. Phys. 7 (2005). <http://www.iop.org/EJ/abstract/1367-2630/7/1/E03>
- [7] T.G. Mackay, A. Lakhtakia, Negative refraction in outer space, Curr. Sci. 86 (2004) 1593.
- [8] T.G. Mackay, A. Lakhtakia, Negative phase velocity in a uniformly moving, homogeneous, isotropic, dielectric-magnetic medium, J. Phys. A: Math. Gen. 37 (2004) 5697–5711.
- [9] T.G. Mackay, A. Lakhtakia, Orthogonal-phase-velocity propagation of electromagnetic plane waves, (2005). <http://arxiv.org/abs/physics/0511210>
- [10] H.C. Chen, Theory of Electromagnetic Waves, McGraw-Hill, New York, NY, USA, 1983, Chap. 8.
- [11] C.H. Pappas, Theory of Electromagnetic Wave Propagation, Dover Press, New York, NY, USA, 1988, Chap. 7.
- [12] B.R. Chawla, H. Unz, Electromagnetic Waves in Moving Magneto-plasmas, University Press of Kansas, Lawrence, KS, USA, 1971.



- [13] F.J. Rachford, D.L. Smith, P.F. Loschialpo, D.W. Forester, Calculations and measurements of wire and/or split-ring negative index media, *Phys. Rev. E* 66 (2002) 036613.
- [14] C.R. Simovski, S. He, Frequency range and explicit expressions for negative permittivity and permeability for an isotropic medium formed by a lattice of perfectly conducting  $\Omega$  particles, *Phys. Lett. A* 311 (2003) 254–263.
- [15] N.C. Paniou, R.M. Osgood, Numerical investigation of negative refractive index metamaterials at infrared and optical frequencies, *Opt. Commun.* 223 (2003) 331–337.










	$\theta = 165^\circ$
	$\theta = 145^\circ$
	$\theta = 125^\circ$
	$\theta = 105^\circ$
	$\theta = 85^\circ$
	$\theta = 65^\circ$
	$\theta = 45^\circ$
	$\theta = 25^\circ$
	$\theta = 5^\circ$

Table 1. Key for the values of  $\theta$  used in Figures 1 and 2.

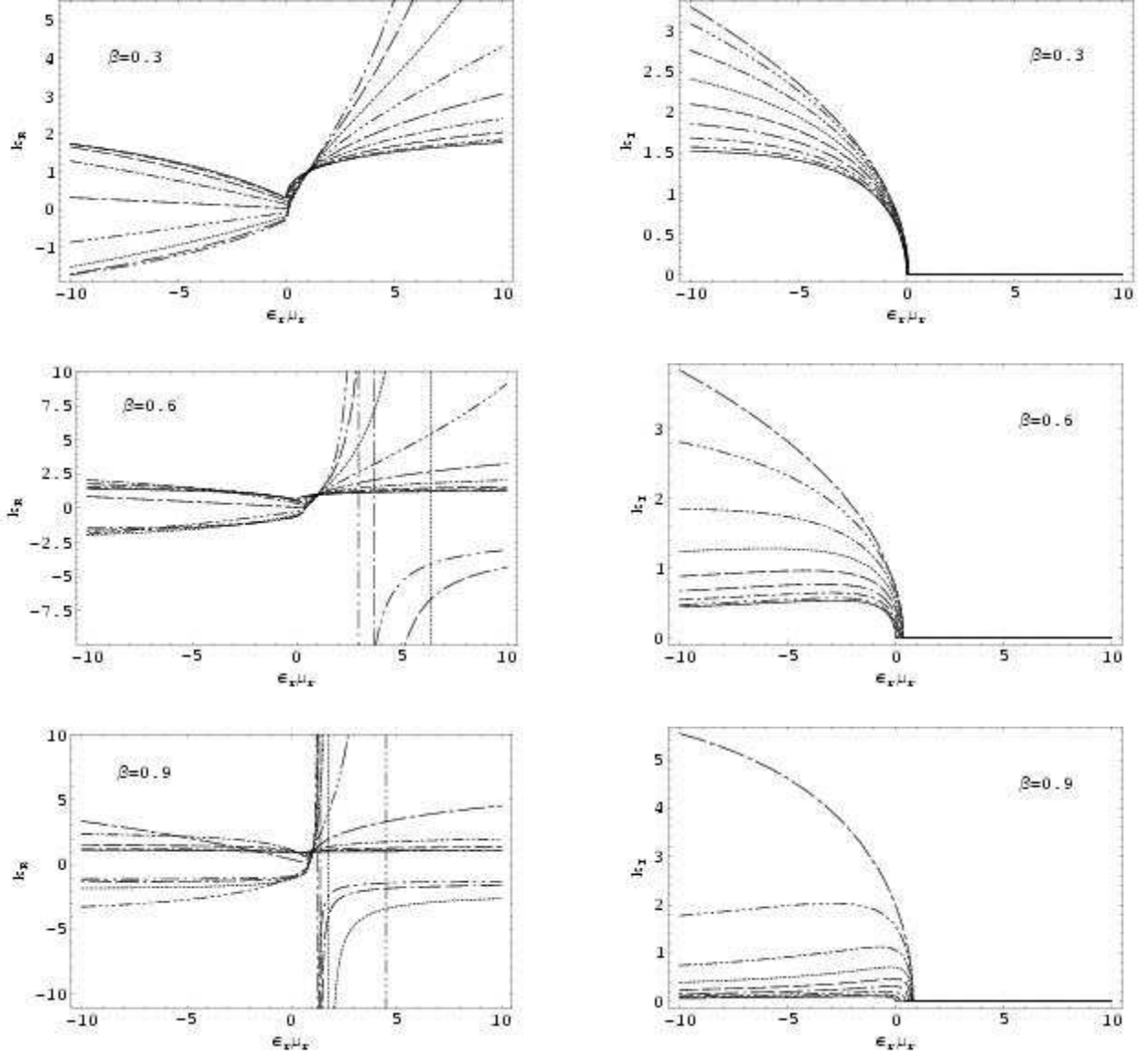


Figure 1: The real (left) and imaginary (right) parts of the wavenumber  $k$  for nondissipative mediums, normalized with respect to  $k_0$ , plotted against  $\epsilon_r \mu_r$  for  $\beta \in \{0.3, 0.6, 0.9\}$ . The values of  $\theta$  are identified in Table 1.

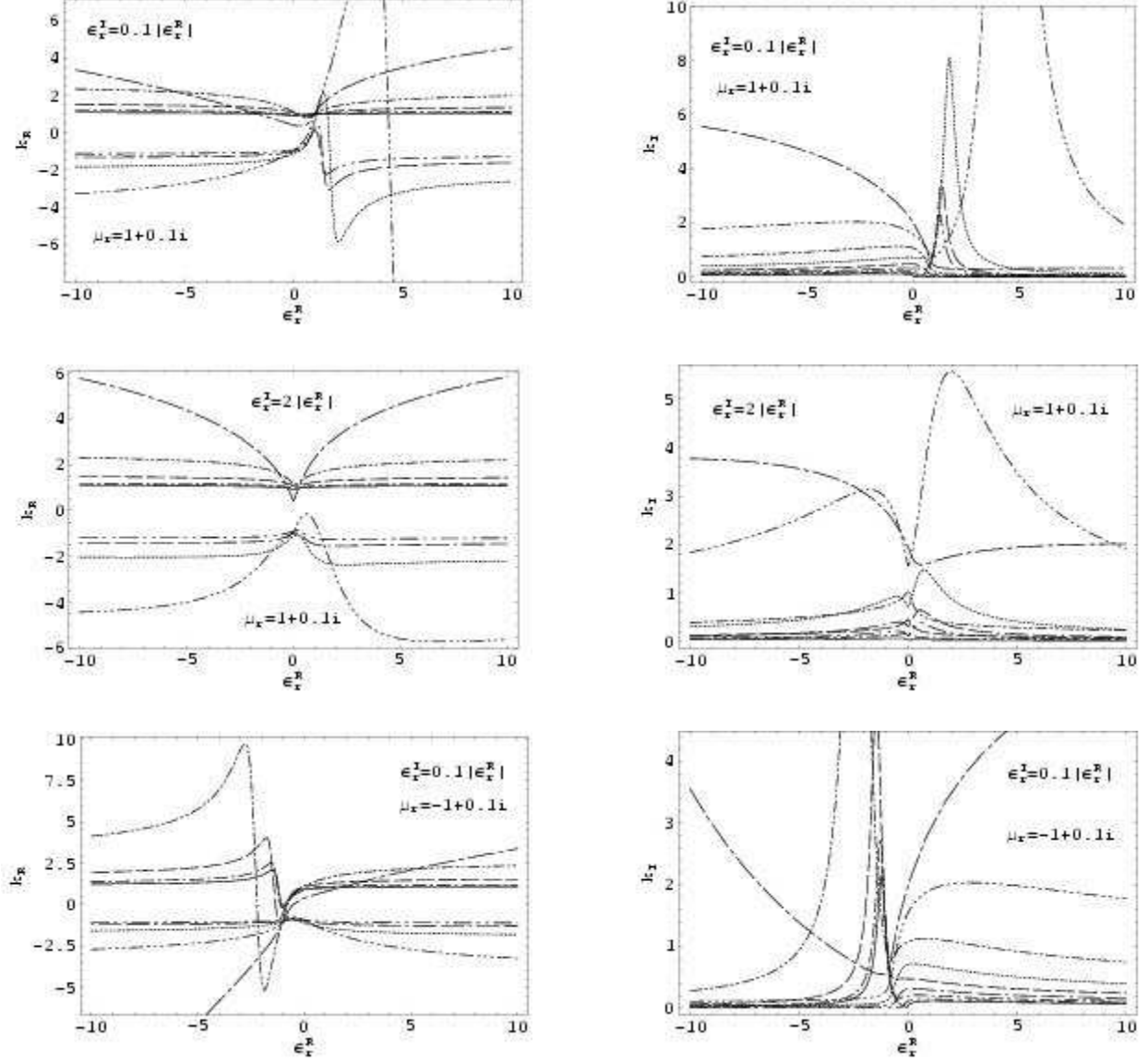


Figure 2: The real (left) and imaginary (right) parts of the wavenumbers  $k$  for dissipative mediums, normalized with respect to  $k_0$ , plotted against  $\epsilon_r^R$  for  $\epsilon_r^I \in \{0.1|\epsilon_r^R|, 2|\epsilon_r^R|\}$ ,  $\mu_r = \pm 1 + 0.1i$ , and  $\beta = 0.9$ . The values of  $\theta$  are identified in Table 1.

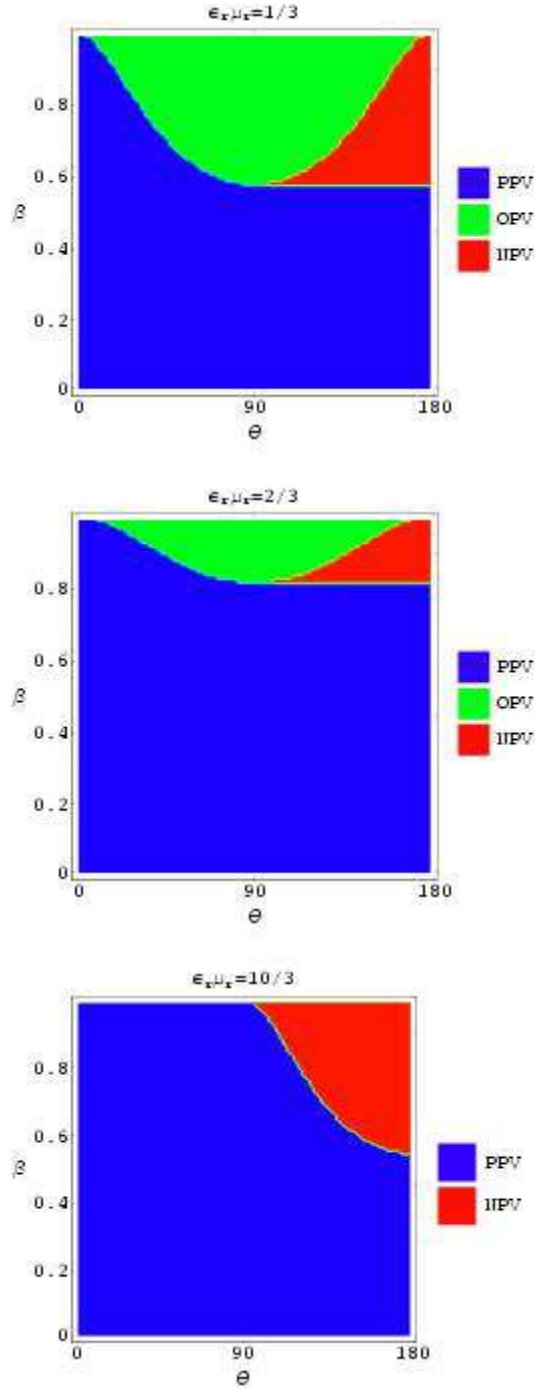


Figure 3: The distribution of positive phase velocity (PPV), negative phase velocity (NPV), and orthogonal phase velocity (OPV), in relation to  $\beta \in (0, 1)$  and  $\theta \in (0^\circ, 180^\circ)$  when  $\epsilon_r \mu_r = 1/3, 2/3$ , and  $10/3$ . The labels ‘NPV’ and ‘PPV’ shown hold for  $\epsilon_r > 0$  and  $\mu_r > 0$ , but must be reversed for  $\epsilon_r < 0$  and  $\mu_r < 0$ .

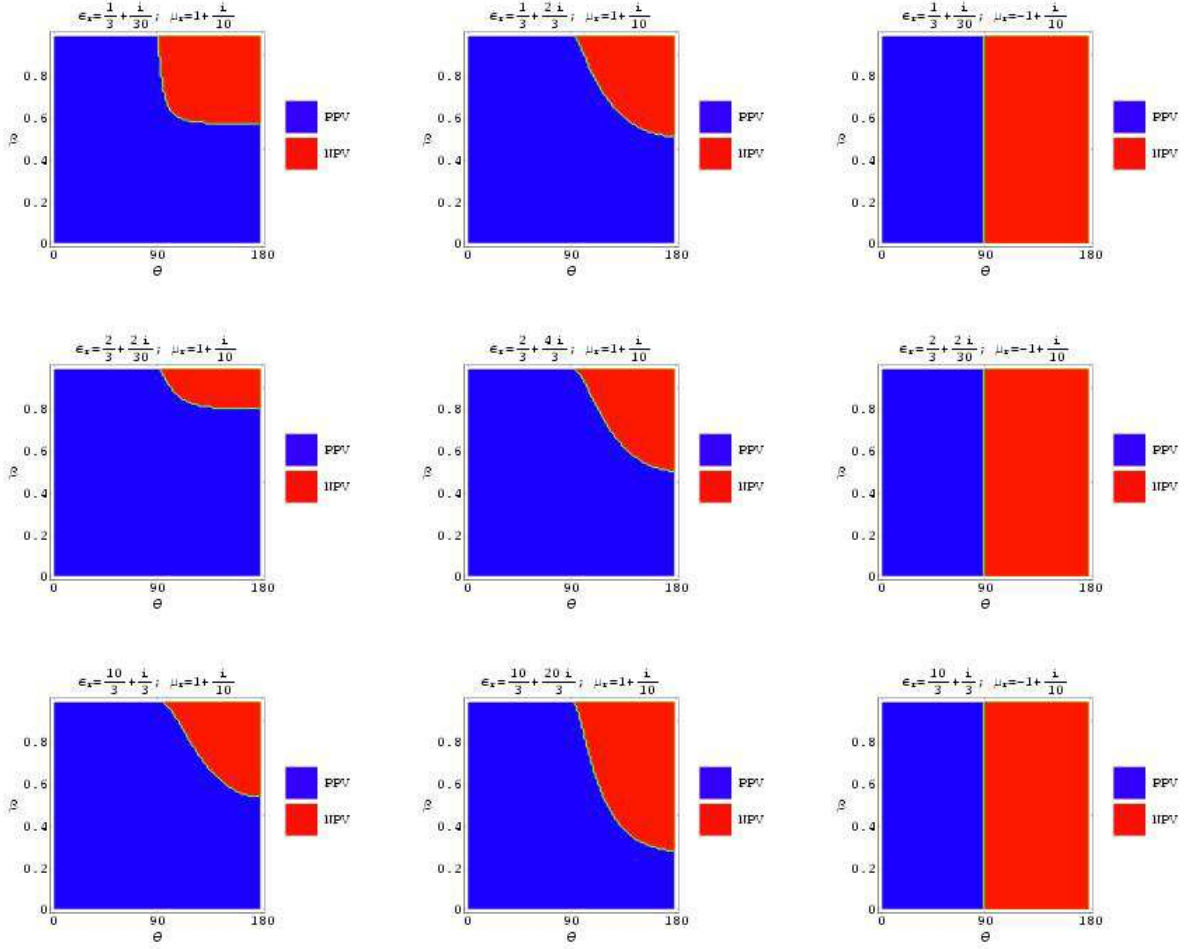


Figure 4: The distribution of positive phase velocity (PPV) and negative phase velocity (NPV) in relation to  $\beta \in (0, 1)$  and  $\theta \in (0^\circ, 180^\circ)$ , for  $\epsilon_r^R \in \{\pm 1/3, \pm 2/3, \pm 10/3\}$ ,  $\epsilon_r^I \in \{0.1\epsilon_r^R, 2|\epsilon_r^R|\}$ , and  $\mu_r = \pm 1 + 0.1i$ .

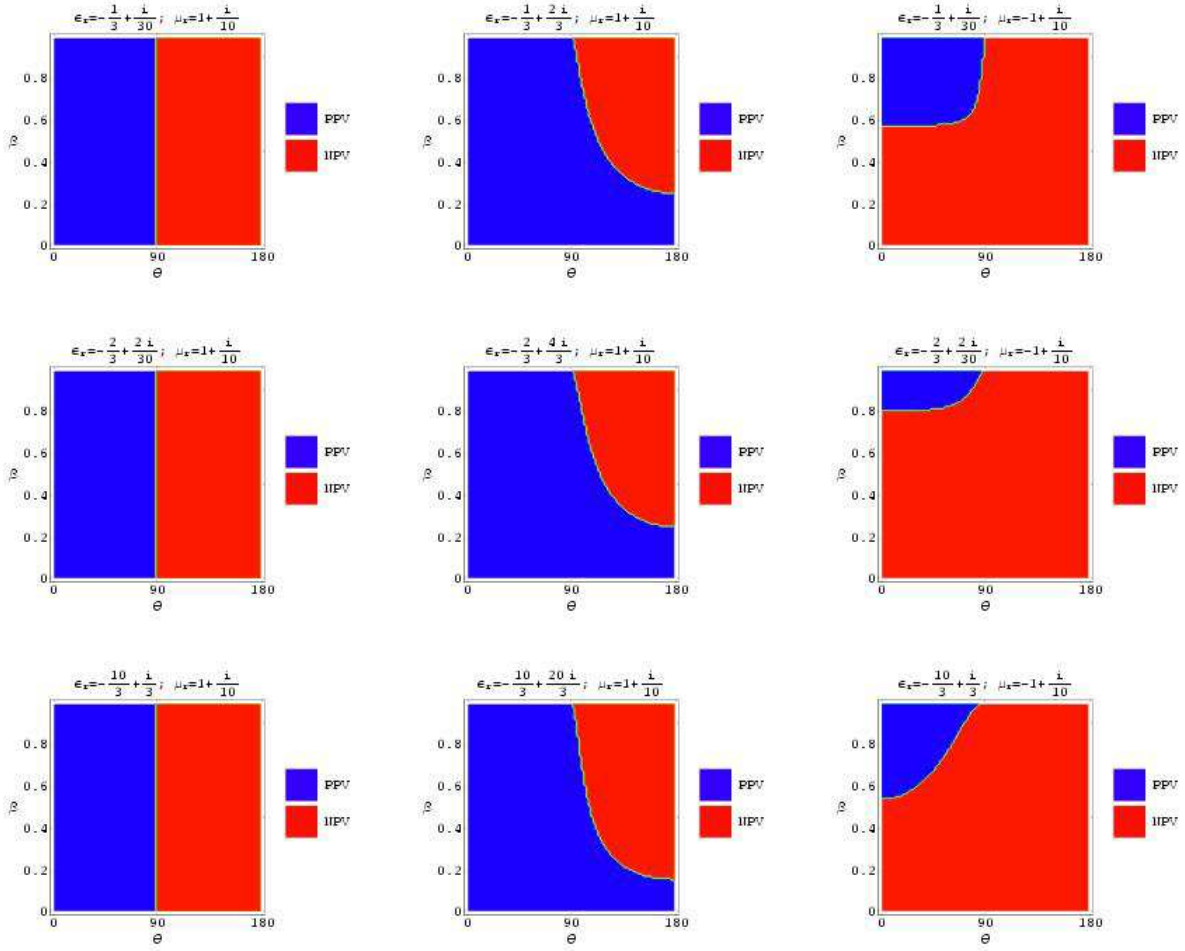


Figure 4: Continued.

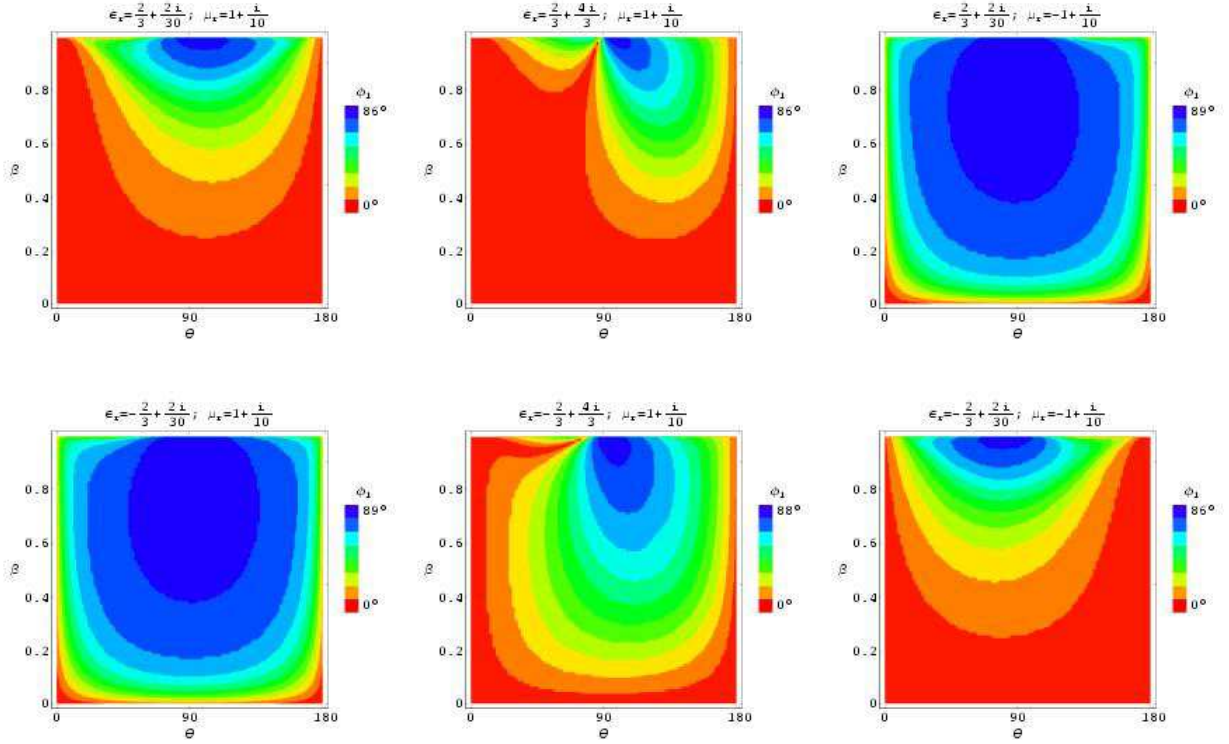


Figure 5: The angles  $\phi_1$  and  $\phi_2$  as functions of  $\beta \in (0, 1)$  and  $\theta \in (0^\circ, 180^\circ)$ , for  $\epsilon_r^R = \pm 2/3$ ,  $\epsilon_r^I \in \{0.1|\epsilon_r^R|, 2|\epsilon_r^R|\}$ , and  $\mu_r = \pm 1 + 0.1i$ .



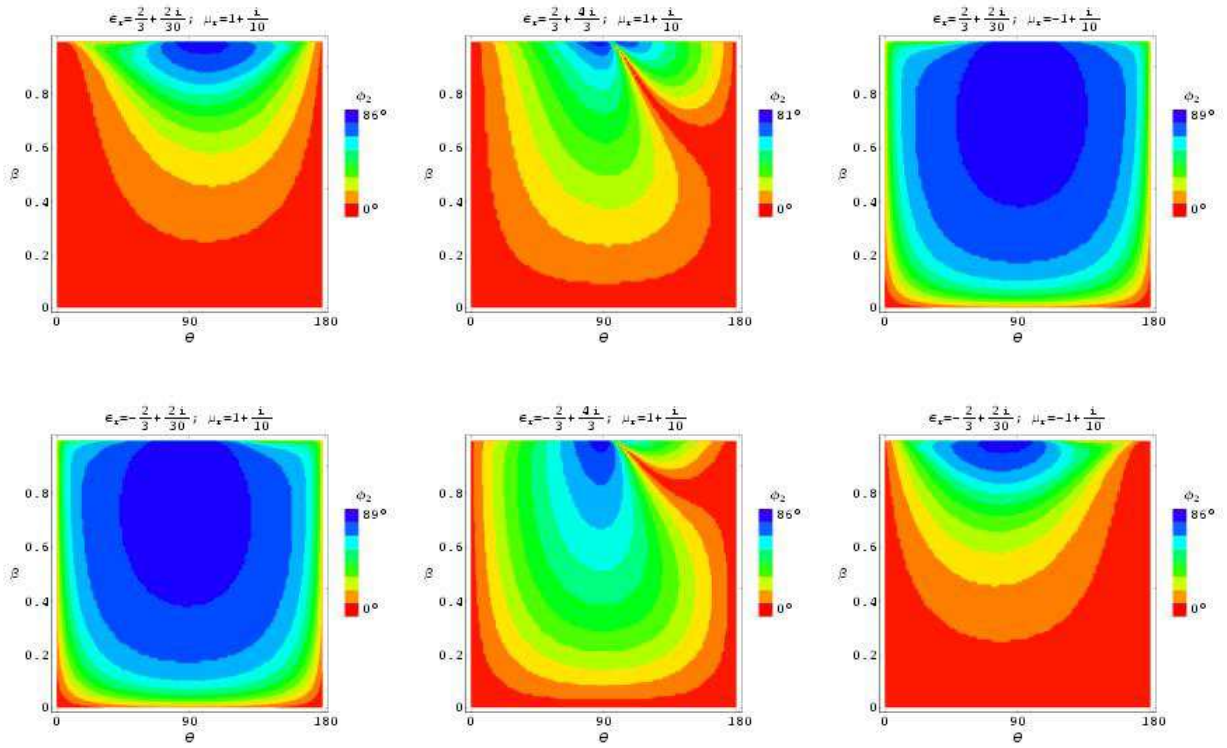


Figure 5: Continued.

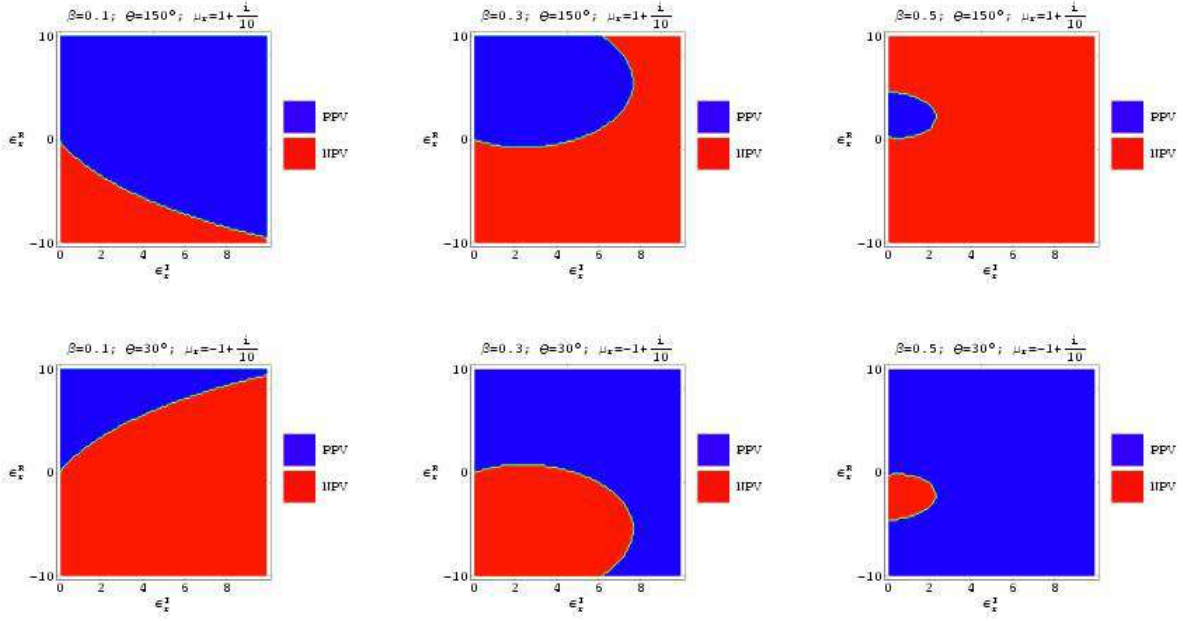


Figure 6: The distribution of positive phase velocity (PPV) and negative phase velocity (NPV) in relation to  $\epsilon_r^R \in (-10, 10)$  and  $\epsilon_r^I \in (0, 10)$ , for  $\theta \in \{30^\circ, 150^\circ\}$ ,  $\beta \in \{0.1, 0.3, 0.5\}$ , and  $\mu_r = \pm 1 + 0.1i$ .

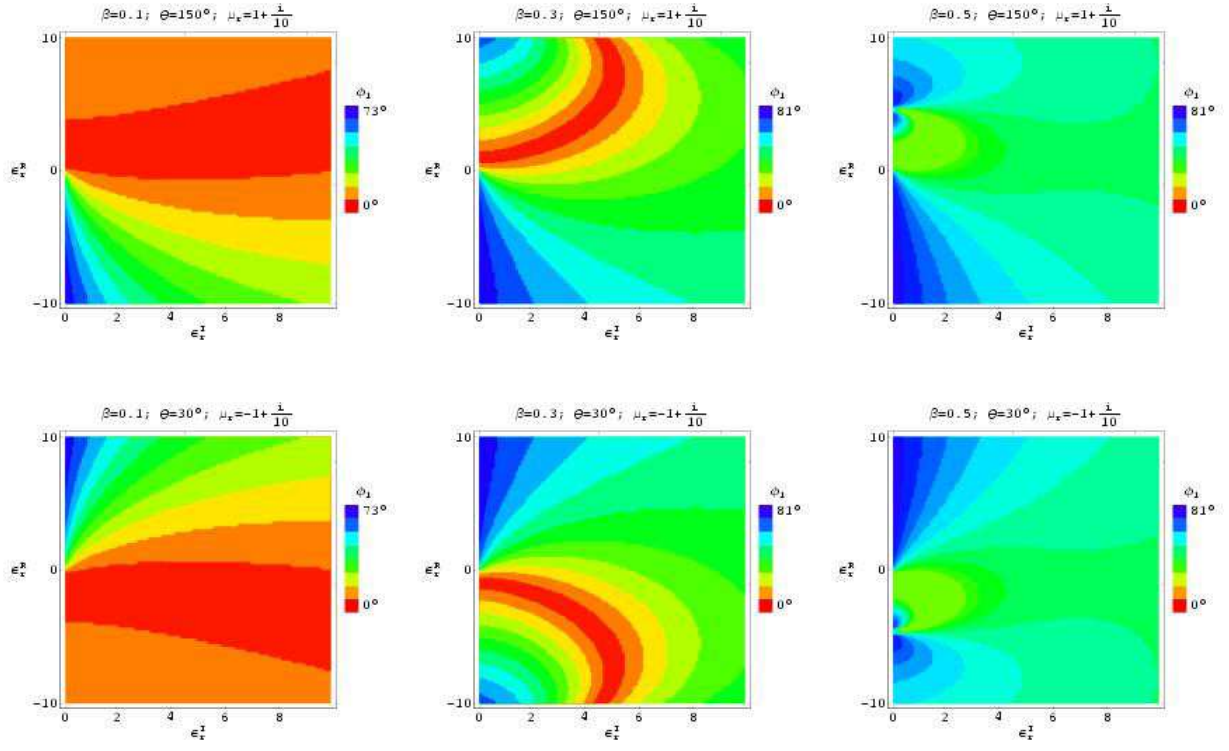


Figure 7: The angles  $\phi_1$  and  $\phi_2$  as functions of  $\epsilon_r^R \in (-10, 10)$  and  $\epsilon_r^I \in (0, 10)$ , for  $\theta \in \{30^\circ, 150^\circ\}$ ,  $\beta \in \{0.1, 0.3, 0.5\}$ , and  $\mu_r = \pm 1 + 0.1i$ .

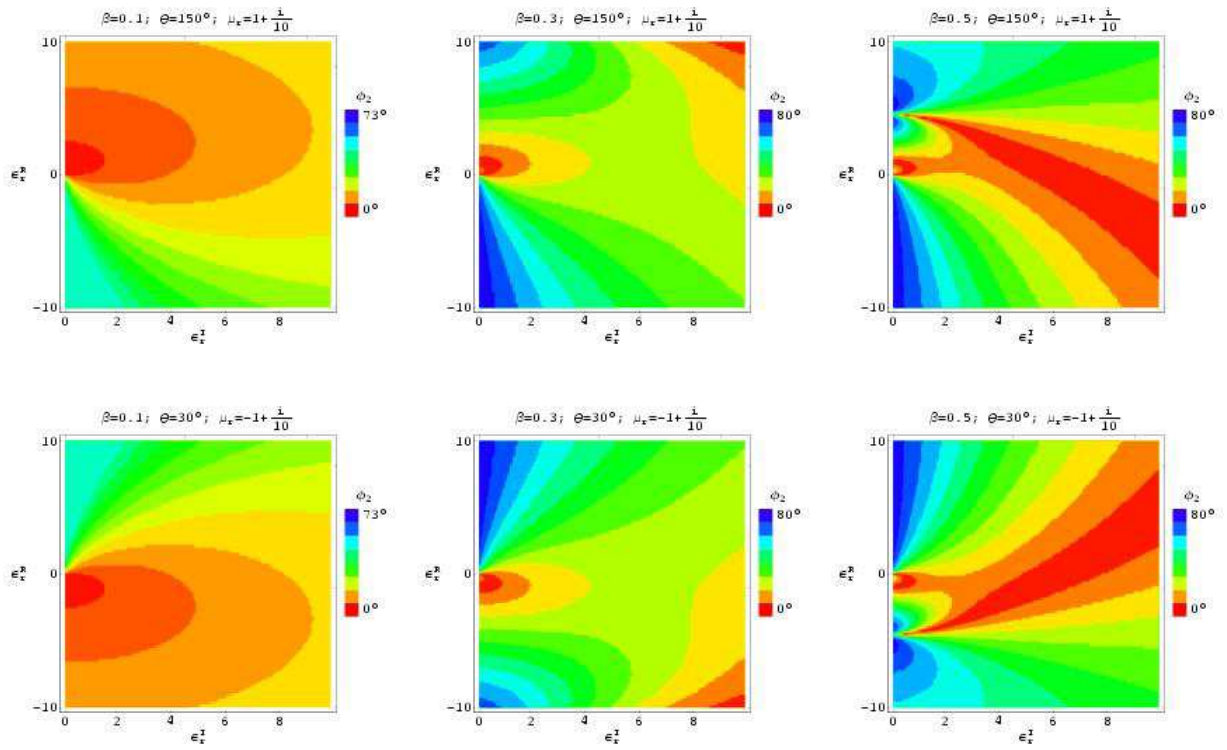


Figure 7: Continued.